Monitoring fatigue crack growth using nonlinear ultrasonic phased array imaging

2017 Smart Mater. Struct. 26 055006

(http://iopscience.iop.org/0964-1726/26/5/055006)

OPEN ACCESS
IOP Publishing
Smart Materials and Structures
Smart Mater. Struct. **26** (2017) 055006 (10pp)
https://doi.org/10.1088/1361-665X/aa6787

Monitoring fatigue crack growth using nonlinear ultrasonic phased array imaging

Jingwei Cheng, Jack N Potter, Anthony J Croxford and Bruce W Drinkwater

Department of Mechanical Engineering, University of Bristol, Queen's Building, University Walk, Bristol BS8 1TR, United Kingdom

E-mail: jingwei.cheng@bristol.ac.uk

Received 30 November 2016, revised 10 March 2017
Accepted for publication 17 March 2017
Published 10 April 2017

Abstract

Nonlinear imaging techniques have recently emerged which have the potential to detect material degradation and challenging defects, such as closed cracks. This paper describes an investigation into the performance of nonlinear ultrasonic imaging (NUI) for the monitoring of the early stages of fatigue crack growth. This technique, in conjunction with conventional array imaging, is applied to the periodic monitoring of steel compact tension specimens subjected to high cycle fatigue loading. The detection limits of these techniques are investigated. Their abilities to localise and detect small cracks are further quantified with the aid of micrography. The results suggest that NUI is more sensitive than conventional ultrasonic imaging to the microscale changes occurring at the early stages of failure, i.e. detectability starts c. 15% of fatigue life. In addition to early detection, the potential for NUI to deliver accurate sizing of fatigue cracks and monitor crack propagation is also presented.

Keywords: monitoring, fatigue crack, ultrasonic phased array, nonlinear imaging

(Some figures may appear in colour only in the online journal)

1. Introduction

Crack growth generated by fatigue loading causes the failure of many aged engineering structures. Early detection is therefore important to plan maintenance and guarantee the safety of structures. Conventional ultrasonics using various arrangements of transmitting and receiving transducers represents a suite of approaches to crack detection and sizing that are widely used in industry. However, it is well known that these techniques are inaccurate if the crack is small or partially closed [1–3]. This means that the detection of fatigue in its early stages is not currently possible and necessarily non-destructive inspection is focussed on monitoring cracks towards the middle and end of a component's fatigue life. The consequence is that inspection intervals must be shortened and/or designs must have higher margins of safety, reducing structural efficiency and adding cost.

Nonlinear ultrasonic techniques have shown the potential to detect cracks at a much earlier stage and have sensitivity to partially-closed defects [4, 5]. Work [6–10] has considered the use of harmonic generation and frequency modulation to identify the nonlinear components of signals reflected from fatigue cracks. However, despite significant research efforts [11–26] these techniques have yet to become accepted by industry. This is in part due to the impracticality of the complicated bespoke setups required for the localisation of elastic nonlinearity. Recent advances have however enabled nonlinear phased array imaging, allowing nonlinearity to be isolated spatially whilst requiring a similar experimental setup to conventional linear array imaging.

The present paper uses an off-the-shelf phased array to create much higher resolution nonlinear images than was previously possible. In addition a diffuse field nonlinear metric is explored and shown to have high sensitivity to the nonlinear signals. More specifically, the paper builds on the recently developed nonlinear ultrasonic imaging (NUI)

technique [27] and explores its potential for early crack detection and monitoring. The NUI technique uses an array to create a spatial map of nonlinearity by focusing on each pixel in the image. The array is used to focus in two modes: *parallel*, in which the elements are fired near simultaneously with an applied delay law, resulting in high intensity focus at the pixel location; and *sequential* in which the elements are fired separately and the interference effects of focusing achieved synthetically through a post-processing operation. The two resulting fields would be identical if linear superposition held and so any differences can be used as a measure of nonlinearity. Importantly, this difference is also insensitive to other sources of nonlinearity such as instrumentation nonlinearity and nonlinear contact-acoustic effects at the array-specimen interface as these occur before the ultrasound interacts with the sample. The imaging metric used is the difference in statistical diffuse energy for fields generated through sequential and parallel focusing at each pixel location. In this context, the diffuse acoustic regime is that which is created after long times in which the ultrasonic waves are spatially uncorrelated and uniformly distributed in the sample. Previous work described NUI [27] and showed its potential for the detection of small defects within aluminium specimens. In the present paper we explore its sensitivity to very small defects within noisier materials (e.g. mild steel) and quantify the earliest point at which detection is achieved in a fatigue test. We also explore the accuracy of crack sizing achievable. The NUI technique is implemented alongside a conventional linear imaging technique, termed total focusing method (TFM) [28] for comparison purposes. Indeed, we show that the same array used with a standard commercially available array controller can be used to produce co-located linear and nonlinear images. In this way, the nonlinear image can be seen as providing complementary information, which can be used in conjunction with the conventional linear information.

2. Linear (TFM) and nonlinear (NUI) imaging

In a typical commercially available array controller two alternative modes of operations are possible. In parallel mode, independently controlled circuits allow the firing of transmitter elements in a pre-set sequence termed a delay law. Similarly these, or other, delays can be applied to the received signals on reception to form an image. The use of this mode of parallel firing and delays on transmission results in a high intensity beam forming in the specimen that can be controllably translated, steered or focused. Alternatively, sequential transmission and capture can be used and the time-domain signals from all the individual combinations of transmitter–receiver pairs captured one after the other. This so called full matrix capture (FMC) [28] data can then be post-processed to form an image. The key difference here is that, as the signals from individual elements are transmitted separately, in this sequential mode the high amplitude focus is not physically generated in the sample. If the test structure is time invariant and the principle of linear superposition holds, these two modes of operation yield identical images.

The NUI technique capitalises on the physical difference in amplitude of the waves at the focal point if the parallel and sequential modes are compared. It is apparent that the pressure amplitude, A, at the focus, is of the order of N times higher in the parallel case, where N is the number of elements in the array. Considering the case of classical third order strain energy, since the amplitude of any second harmonic wave generated is proportional to A^2 and the energy of the wave is proportional to A^2, the amount of energy in the second harmonic wave, is proportional to A^4. Furthermore, since the energy is conserved, the amount of energy lost from the fundamental will be N^3 times higher in the parallel case. Note that in practice higher harmonics could exist and these would result in further energy loss from the fundamental. In the NUI technique the energy in the fundamental is measured as the integral of A^2 over some time window which is set to be within the diffuse field, i.e. at a time after which the energy is uniformly distributed within the sample.

The requirement to measure the energy of the diffuse field means that the selection of reception start time t_r (the time instant when each element starts to receive signals) and window length T (the time length corresponding to duration of the time domain signal each receiver acquires) is particularly important. There are two competing effects. First, the acoustic field only slowly tends to the diffuse field condition with time. Second, as wave propagation is dissipative, the signal-to-noise ratio will decrease with time. Ultimately, compromise values of t_r and T must be found such that a diffuse field condition is achieved and the amplitude is acceptable, i.e. the signal-to-noise ratio is sufficient.

Assuming $f_{n,m}(t)$ are the time-domain received signals for each combination of transmit (n) and receive (m) elements in the sequential case. $\delta_n(\boldsymbol{r})$ is the transmission delay applied to the nth element to achieve a focus at a point $\boldsymbol{r}$. Also, $h_m(\boldsymbol{r}, t)$ is the time-domain signal received on element m for the parallel transmission of all elements delayed independently by $\delta_n(\boldsymbol{r})$. The frequency (ω) domain versions of $f_{n,m}(t)$ and $h_m(\boldsymbol{r}, t)$ are given by $F_{n,m}(\omega) = \int_{t_r}^{t_r+T} f_{n,m}(t)\mathrm{e}^{-\mathrm{i}\omega t}\mathrm{d}t$ and $H_m(\omega) = \int_{t_r}^{t_r+T} h_m(t)\mathrm{e}^{-\mathrm{i}\omega t}\mathrm{d}t$, respectively.

The energy content of the fundamental is then found from integration of the amplitude squared across the frequency domain from $\frac{2}{3}\omega_0$ to $\frac{4}{3}\omega_0$. These integration limits are chosen to exclude nonlinear energy flux within the evaluated bandwidth. Consequently, the diffuse acoustic energy in the sequential focusing case E_s at focal point, $\boldsymbol{r}$, for an N element array is given as:

$$E_s(\boldsymbol{r}) = \sum_{m=1}^{N}\left(\int_{\frac{2}{3}\omega_0}^{\frac{4}{3}\omega_0} \omega^2 \left|\sum_{n=1}^{N} F_{n,m}(\omega)\mathrm{e}^{\mathrm{i}\omega\delta_n(\boldsymbol{r})}\right|^2 \mathrm{d}\omega\right). \quad (1)$$

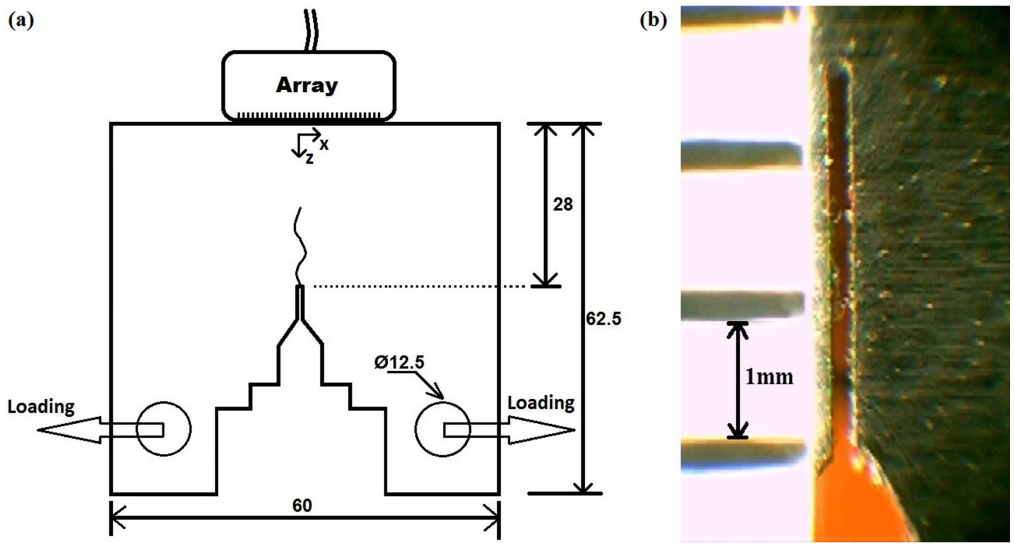

Figure 1. (a) Schematic diagram of nonlinear and linear phased array measurement configuration on CT specimen (dimensions in mm) and (b) photograph (zoomed in with a millimetre scale) of the 0.1 mm wide notch on the CT specimen before fatigue test.

Likewise, the parallel transmission energy E_p is calculated as follows:

$$E_p(\boldsymbol{r}) = \sum_{m=1}^{N}\left(\int_{\frac{2}{3}\omega_0}^{\frac{4}{3}\omega_0} \omega^2 \, |H_m(\boldsymbol{r}, \omega)|^2 \mathrm{d}\omega\right). \quad (2)$$

Finally an image is formed by calculation of the nonlinear metric γ at a given imaging/focal point $\boldsymbol{r}$ [27]

$$\gamma(\boldsymbol{r}) = \frac{E_s(\boldsymbol{r}) - E_p(\boldsymbol{r})}{E_s(\boldsymbol{r})}. \quad (3)$$

The nonlinear metric γ at every focal point $\boldsymbol{r}$ is used to produce a full nonlinear image in the x–z plane (see figure 1(a) for axis definition). Alongside this a conventional TFM image of the same size is produced in order to visualise the linear features of the specimen, which the nonlinear imaging technique cannot display. The TFM image, $I(x, z)$, is given by:

$$I(x, z) = \left|\sum g_{n,m}\left(\frac{\sqrt{(x_n - x)^2 + z^2} + \sqrt{(x_m - x)^2 + z^2}}{c}\right)\right|, \quad (4)$$

where $g_{n,m}$ is the Hilbert transform of, $f_{n,m}$, the position of focal point $\boldsymbol{r}$ is defined in terms of x and z coordinates, c is the speed of sound and the summation is performed over all transmitters and receivers.

3. Experimental procedure

Mild steel ASTM A36 ($c = 5924\ \mathrm{m\,s^{-1}}$) compact tension (CT) specimens were manufactured according to the ASTM standard E647-05. The load limits were then selected to ensure that the specimen failed in the high cycle fatigue regime. The maximum stress intensity factor K_{max} was chosen as:

$$K_{max} = \frac{K_{IC}}{3}, \quad (5)$$

where $K_{IC} = 65\ \mathrm{MN\,m^{-3/2}}$ is the nominal fracture toughness of this material. The minimum stress intensity factor K_{min}, using a stress ratio value of $R = 0.13$ (where the stress ratio R is the ratio of the minimum and maximum load, P_{min} and P_{max}, per cycle), is calculated below:

$$K_{min} = RK_{max} = \frac{P_{min}}{P_{max}}K_{max}. \quad (6)$$

Complying with ASTM standard E647-05, the geometry factor of the CT specimen is known, and hence the stress intensity factor range ΔK can be expressed as:

$$\Delta K = \frac{\Delta P}{B\sqrt{W}}\frac{(2+\alpha)}{(1-\alpha)^{\frac{3}{2}}}(0.886 + 4.64\alpha - 13.32\alpha^2 + 14.72\alpha^3 - 5.6\alpha^4), \quad (7)$$

where $\Delta P = P_{max} - P_{min}$, B is the thickness of the specimen (25 mm) and $\alpha(= a/W)$ is the ratio of the distance from the load bearing point to the crack tip ($a = 22$ mm), and the width of CT specimen ($W = 50$ mm).

Consequently, the load was varied between 2 and 15 kN (P_{min} and P_{max}) in a hydraulic testing machine (Instron 8800MJ6272, UK) at a frequency of 3 Hz. Furthermore, once the test was stopped after a prescribed number of cycles, metallographic preparation was completed around the crack tip by fine grinding using silicon carbide paper as well as further fine polishing using polishing cloth with a 3 μm monocrystalline diamond suspension. After polishing to a mirror finish, the microstructure around the tip was observed by a microscope (Zeiss Axio Imager 2, Germany) and hence the crack length was monitored periodically during the fatigue test.

The ultrasonic inspections using NUI and TFM imaging were made by positioning an array on the top face above the end of notch as shown in figure 1(a). All the inspections were implemented with a 64 element ultrasonic array (Imasonic, France) with nominal centre frequency of 5 MHz, (−6 dB bandwidth 86% of the centre frequency), and pitch of 0.63 mm, as well as an array controller (Peak NDT Micropulse FMC, UK). It should be noted that the reception start time, t_r, depends on the geometry of specimen, random noise and material properties, since the time to reach the diffuse field varies with these. By observing the performance of NUI on the known nonlinear and linear features of this CT specimen during experiments, appropriate parameters for the NUI imaging were chosen as window length, T of 0.12 ms with the reception start time, t_r, at 0.1 ms, providing a compromise between diffusivity and signal to noise ratio. The initial notch was generated by electrical discharge machining to create a stress concentration and is shown in figure 1(b). In addition, the TFM imaging technique was performed on the side of specimen parallel to the crack face. This provides the best case scenario for linear inspection, however we note that this arrangement is often not practically realisable due to access limitations.

4. Experimental results

4.1. Life monitoring

A mild steel CT specimen was subjected to cyclic loading in order to ascertain the performance of NUI and TFM imaging with crack growth. The fatigue test continued until the specimen failed, as indicated by an opening angle, 5°, in order to estimate the life span based on the specified high cycle fatigue loading. This allows linear and nonlinear metrics to be related to the fatigue life in addition to crack size.

Before the start of fatigue test, the specimen was inspected using linear TFM and the NUI technique, shown in figures 2(a) and (b) to understand the background noise level and the characteristics of the baseline geometric features.

The grain structure of mild steel contributes to energy absorption, increasing the effect of incoherent noise on diffuse field measurements as well as generating coherent noise in linear images in comparison to finer grained materials such as aluminium. Therefore, the background levels presented in figures 2(a) and (b), will inevitably mask some nonlinear and linear features and set detection thresholds. It is likely that time-variant perturbations to the system, for example through environmental changes, between parallel and sequential acquisitions also contribute to the nonlinear background levels. Additionally, incoherent noise has a proportionally larger contribution to the, lower amplitude, sequential measurements. This leads to imperfect subtraction of parallel/sequential fields, reducing the ability to suppress linear features (e.g. planar surfaces and large holes), as is evident by the presence of background response coinciding with linear features. As would be expected, the linear TFM image in figure 2(a) shows the linear scattering from the geometric features of the specimen and the amplitude in figure 2(b) gives an indication of how well these features are supressed.

The fatigue experiments were stopped at the completion of 20 000, 30 000, 50 000, 70 000, 90 000 and 130 000 cycles in order to perform the imaging, with eventual failure occurring at 135 500 cycles. Figures 3(a)–(c), cover the period up to 50 000 cycles, which is thought to correspond to crack nucleation and initial growth. In this initial fatigue region the amplitude of the nonlinear metric can be seen to increase relative to the maximum background level with the maximum nonlinearity occurring in the vicinity of the initiation notch. Figures 3(d)–(f) show the position of maximum nonlinearity (indicated by the red cross) moving ahead of the initiation notch, suggesting more extensive cracking. In all cases, it is likely that the nonlinear response observed (up to four times the maximum background level) is predominantly a consequence of contact-acoustic effects [15]. Figure 3(f) shows that at 130 000 cycles the position of maximum nonlinearity has reached 2 mm from the starter notch tip and its amplitude has decreased somewhat relative to earlier points in the fatigue life. This late-life amplitude effect is likely a consequence of the crack beginning to open as the sample nears failure, resulting in fewer contact points and reduced instances of nonlinear contact acoustic effects. The sample failed shortly after commencing cycling beyond 130 000 cycles.

A linear TFM image was performed with the array located on the top of the sample and this revealed no significant changes in linear scattering above the end of the initiation notch throughout the crack growth. This demonstrates a clear example of the NUI technique having increased sensitivity over a high performance traditional linear technique (i.e. TFM).

As shown in figure 4, the relationship between change in the maximum acoustic nonlinearity and fatigue life demonstrates that the acoustic nonlinearity generally increases until it reaches around 70% of fatigue life. Error bars denote a single standard deviation of peak nonlinear amplitude. This standard deviation is calculated for multiple image acquisitions (between 3 and 5) at each sample point, then averaged over all points. The error bars provide a measure of repeatability for a specimen in a given state, but not between different specimens.

4.2. Early detection investigation

The previous study evaluated the efficacy of imaging throughout the whole fatigue life. A further test was conducted in order to more closely study early stages of crack growth and explore the limits of detectability. The loading step was reduced to 5000 cycles in order to ensure the early stage damage is monitored and detection performance could be investigated.

The results in figures 5(a)–(c) demonstrate nonlinear features consistent with those seen in section 4.1. Initially the crack, which was barely visible in figure 6(a), could not be detected with NUI or the TFM technique. The earliest detection was at 20 000 cycles where the maximum

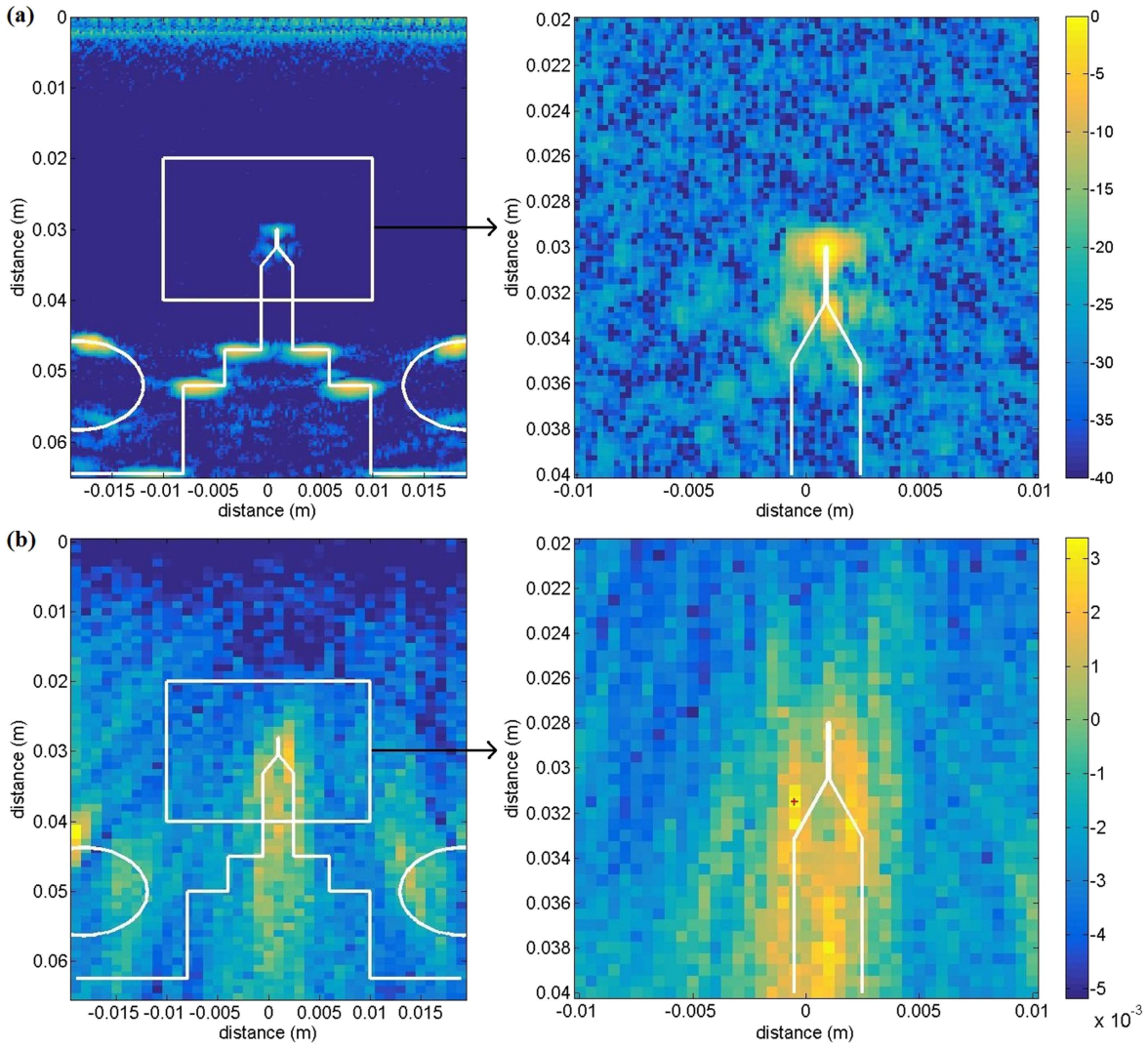

Figure 2. Nonlinear and linear images prior to loading. (a) Linear TFM images on a dB scale (b) nonlinear images of the nonlinear metric, γ.

nonlinearity was near the end of the notch. The micrograph in figure 6(c) was taken at 20 000 cycles and shows that the crack tip was at 251 μm above the initial notch end. The location of the maximum nonlinearity then remained within 1 mm of the crack tip from 20 000 cycles to 40 000 cycles. It should be noted that the fundamental transmitted wavelength is 1.2 mm, which potentially contributes to the error in its localisation. It should also be noted that in this experiment the crack propagation was more likely to generate small branches due to slight variations in loading condition caused by relatively frequent removal and mounting to permit the imaging steps. The branches which might not exist before 40 000 cycles in the previous test may contribute to the small difference in acoustic nonlinearity observed when figures 3 and 5 are compared. Therefore, the difference in the maximum nonlinear metric at the same cycles (from figures 4, 7 and 9) results predominantly from sample-to-sample variations. Figures 5(d) and (e) show the linear TFM images produced through positioning the array at the left side. Despite the advantageous array positioning, the linear array imaging is not able to detect the increase in crack length clearly at 20 000 cycles due to coherent noise and blurring due to the finite point spread function.

Figures 7(a) and (b) show that the maximum nonlinearity at each early fatigue step increases with crack growth from 5000 cycles to 40 000 cycles, which is consistent with the results in section 4.1. It can be seen that the crack tip became detectable from 15% of its fatigue life (20 000 cycles). Here detectability was defined as the first measurement with a lower error bar that exceeded the upper error bar of the zero-load condition. From figure 7(a) this detection limit can be seen to correspond to a crack length of between 200 and 250 μm. It is also worth noting that nearly the whole of figure 7 is below the commonly quoted half-wavelength limit for linear detectability (i.e. 600 μm in this case).

4.3. Sizing analysis

Though not diffraction limited in the classical sense, sub-wavelength geometric features cannot be resolved directly in a nonlinear image. For such features the image produced is that of the associated point spread function for the technique. For this very early stage crack growth, crack size may only be

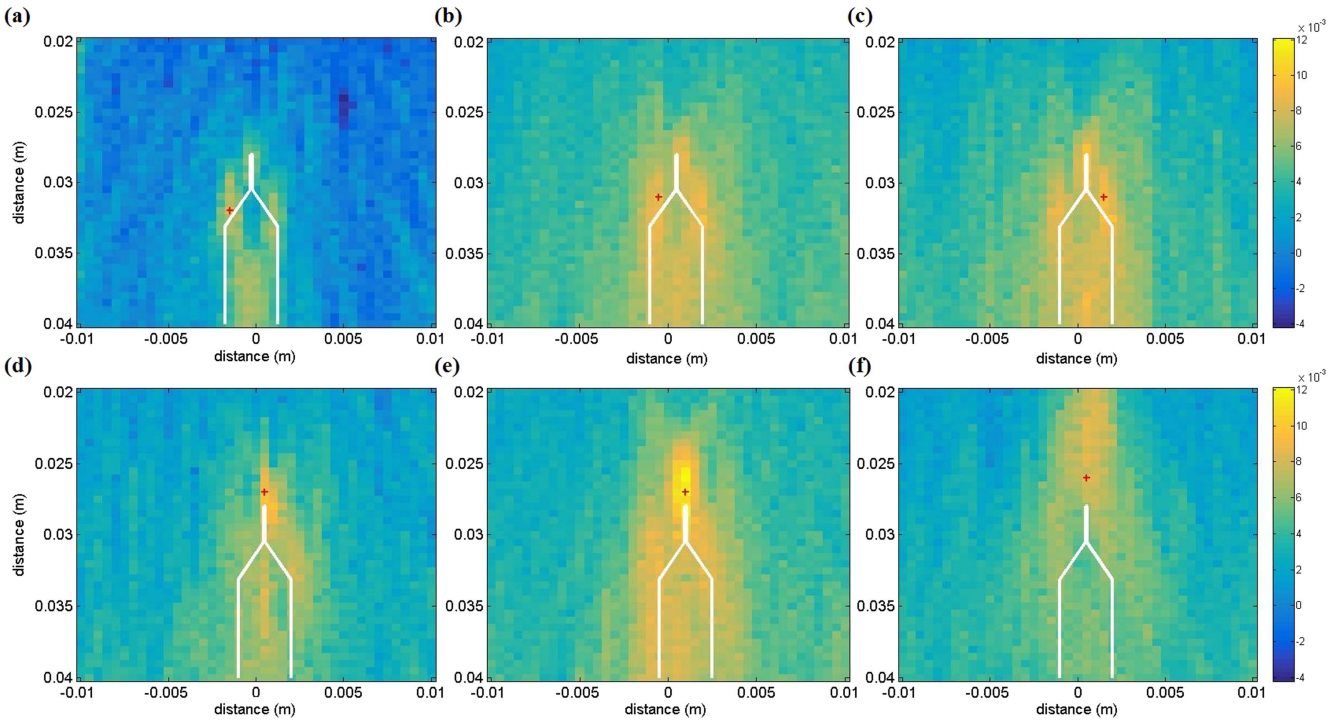

Figure 3. Nonlinear images in nonlinear metric γ at (a) 20 000, (b) 30 000, (c) 50 000, (d) 70 000, (e) 90 000, and (f) 130 000 cycles. Note that the red cross represents position of the maximum γ.

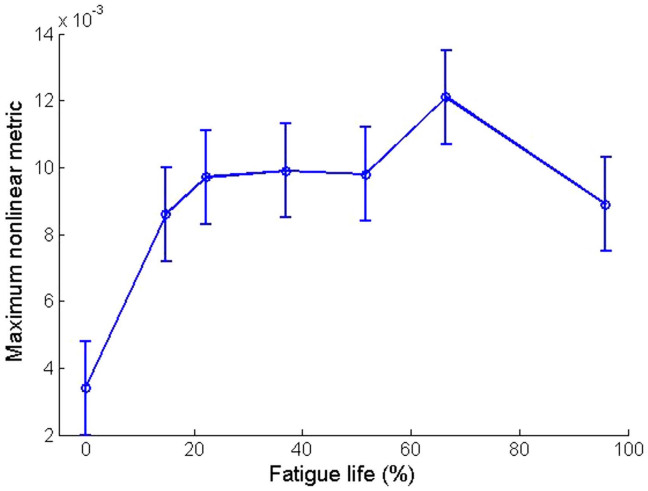

Figure 4. Maximum nonlinear metric, γ, as a function of % fatigue life (error bar represents an averaged standard deviation).

inferred from the amplitude of nonlinear response, as demonstrated in the previous section. As crack length increases beyond the order of half a wavelength, the region of nonlinear contrast within the image increases in size, allowing for direct sizing of defects from nonlinear images.

This section investigates the sizing of small cracks which corresponded here to loading from between 40 000 and 100 000 cycles. Figures 8(a)–(d) show the nonlinear images in this loading range at increments of 20 000 cycles. Noticeably, the maximum magnitude of the nonlinear metric increases almost linearly with crack growth from 40 000 cycles to 100 000 cycles (as shown in figures 9(a) and (b)).

The position of peak nonlinear amplitude and the actual crack tip location as measured from micrographs are indicated in figure 8 as red and black crosses respectively. The location of highest nonlinearity is consistently at approximately 1 mm below the actual crack tip. This is not necessarily indicative of the location of maximum nonlinear response. When focusing at the crack tip, less of the crack lies under the footprint of the focal region, reducing the measured nonlinear response. Aside from this offset, the location of peak nonlinearity is seen to correspond very closely with the actual crack tip location measured from surface micrographs, as is shown in figure 9(c).

5. Conclusions

The experimental results presented show that monitoring fatigue crack growth in mild steel using the NUI technique was effective from 15% fatigue life. The NUI technique was performed using a commercially available array and array controller. The same instrumentation was also used to simultaneously produce traditional high resolution linear TFM images. These linear images did not reveal any detectable changes in these early stages of fatigue. The amplitude of nonlinearity was shown to be a measure of progress of the very early stages of fatigue crack growth. The experiments showed that statistically significant amplitude increases were measureable for cracks of 250 μm length and greater. As crack growth continued the location of maximum nonlinearity was used to measure the extent of the cracking. For these larger cracks the NUI technique becomes a form of nonlinear

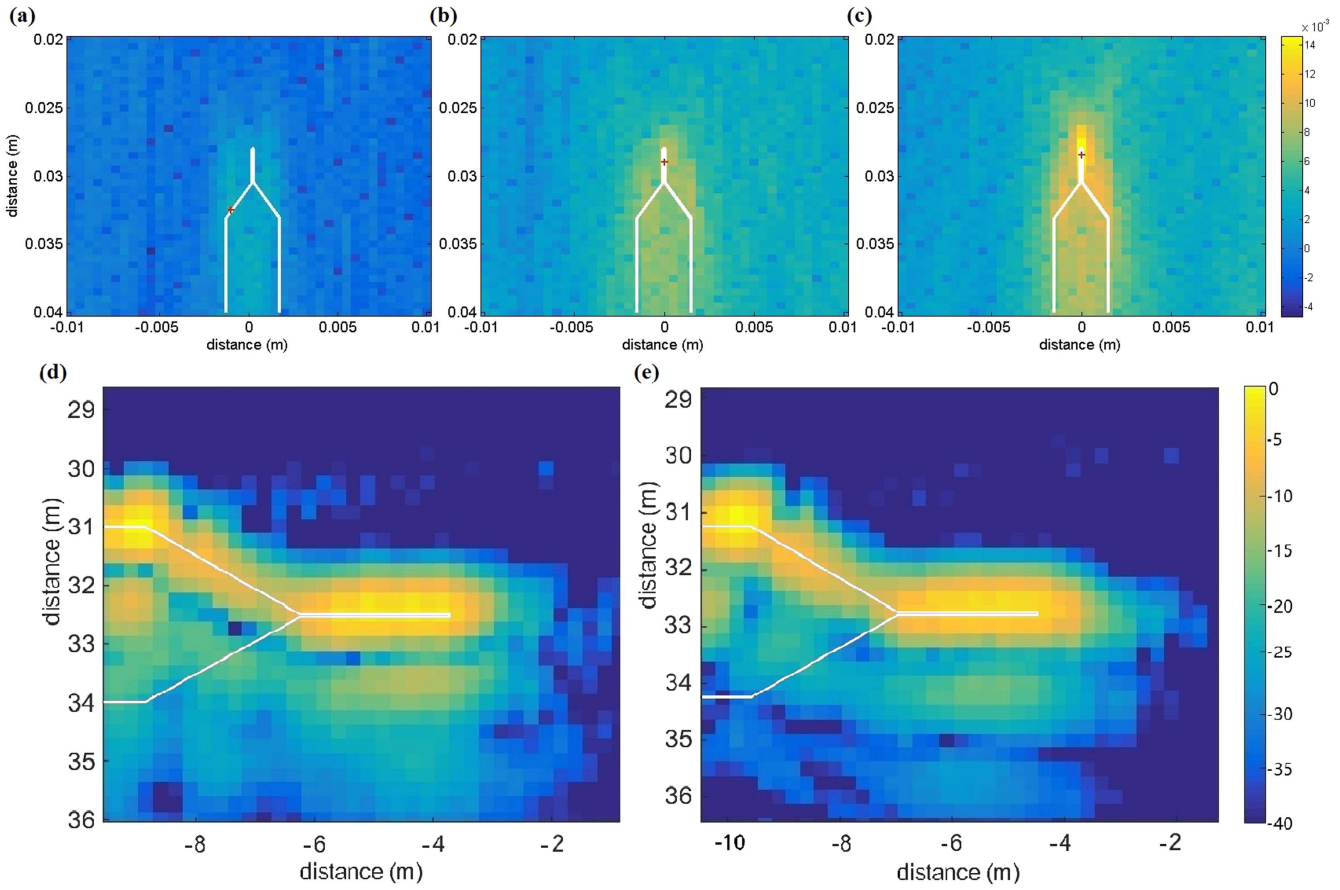

Figure 5. Nonlinear images in nonlinear metric γ at (a) 5000, (b) 20 000 and (c) 40 000 cycles. Note that the red cross represents position of the highest γ. Linear images with array located on the left hand side of the sample at (d) 0 and (e) 20 000 cycles.

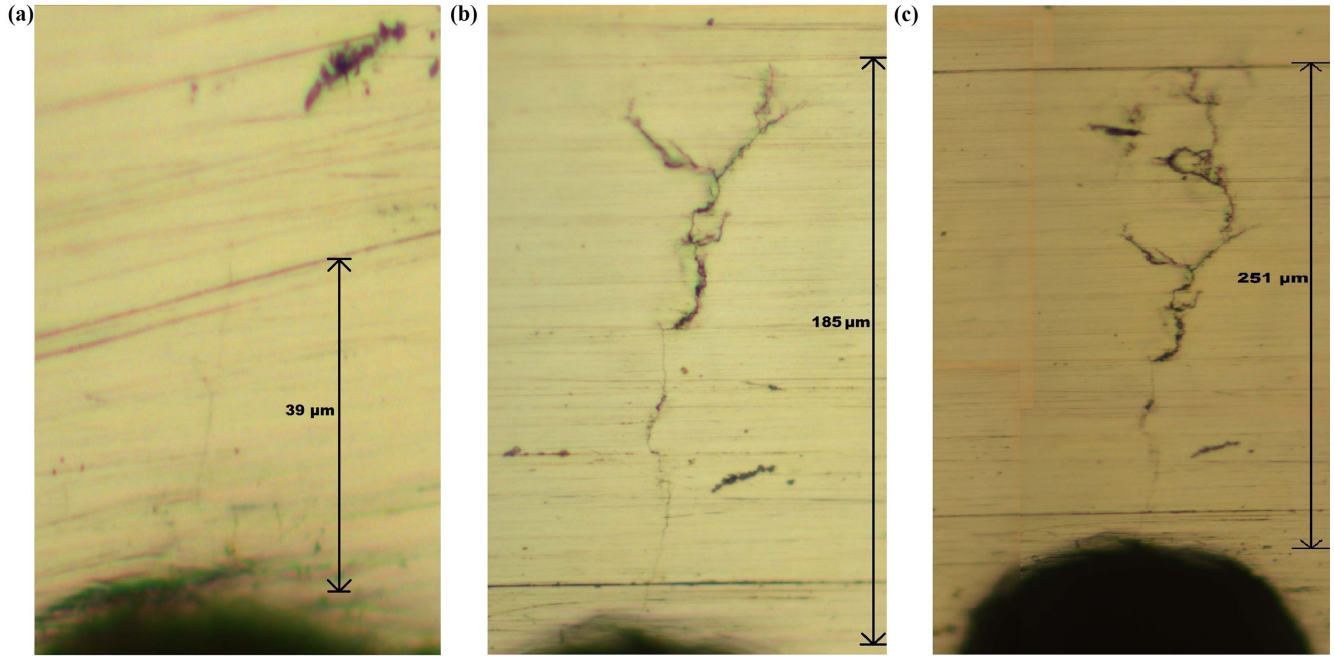

Figure 6. Micrographs of the fatigue crack at (a) 5000, (b) 15 000, and (c) 20 000 cycles. Note that the scale is different in each image.

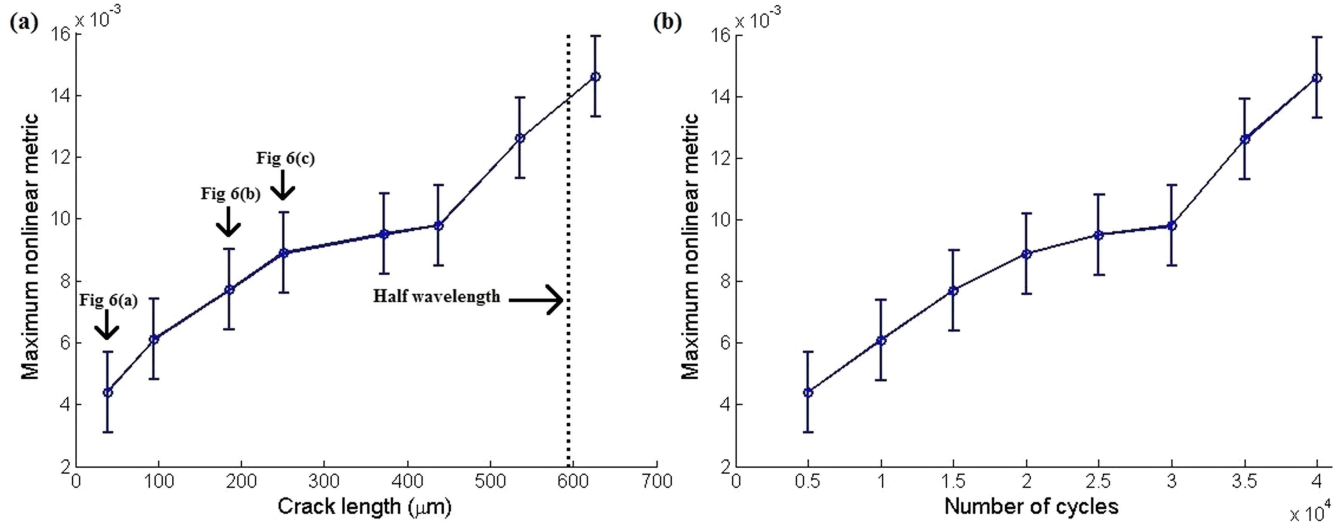

Figure 7. Maximum nonlinear metric γ during fatigue as a function of (a) crack length and (b) number of fatigue cycles (error bars represent an averaged standard deviation).

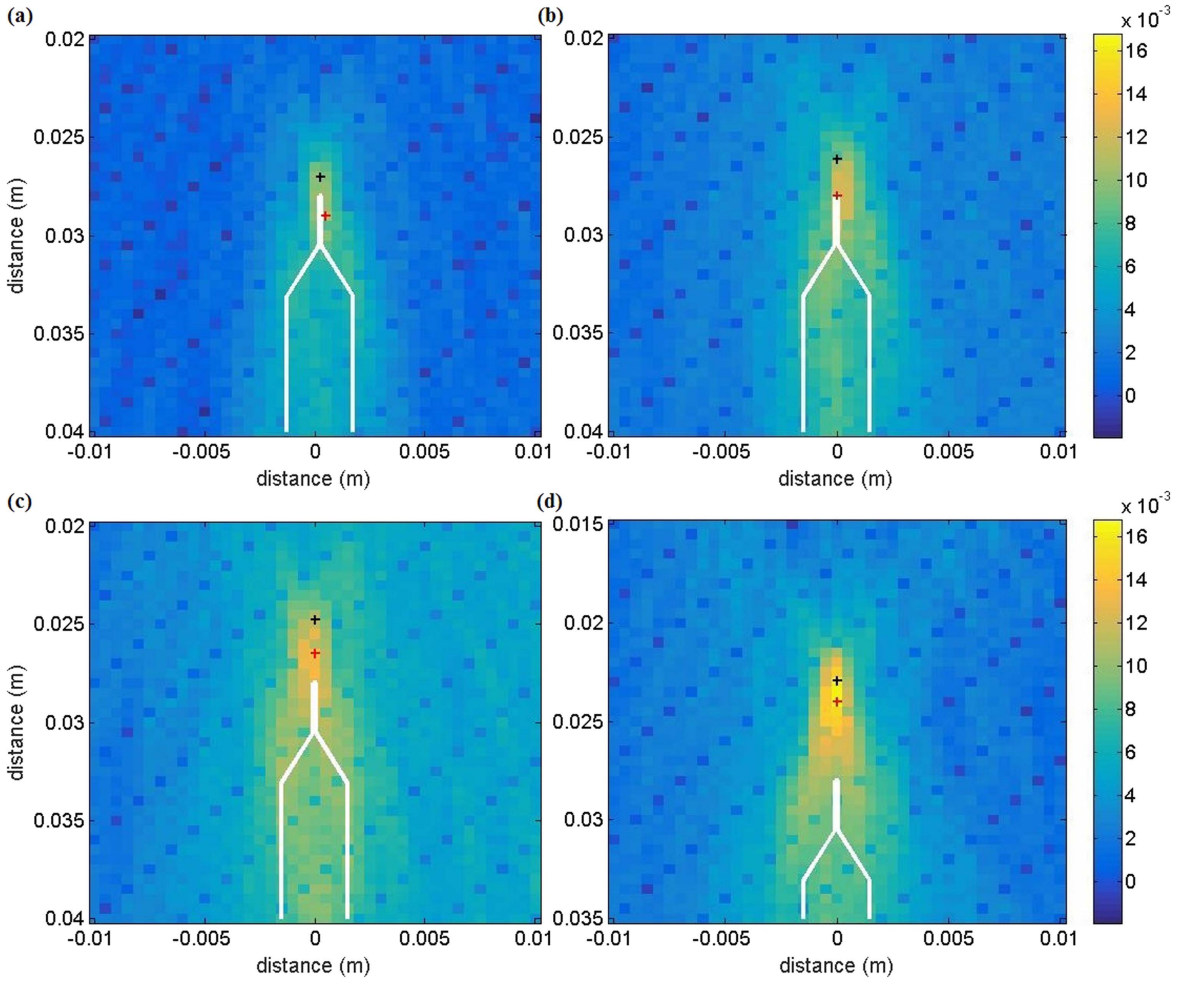

Figure 8. Nonlinear images in nonlinear metric γ at (a) 40 000, (b) 60 000, (c) 80 000, and (d) 100 000 cycles. Note that the red cross and black cross represent positions of the highest γ and the micrographically measured crack tip respectively.

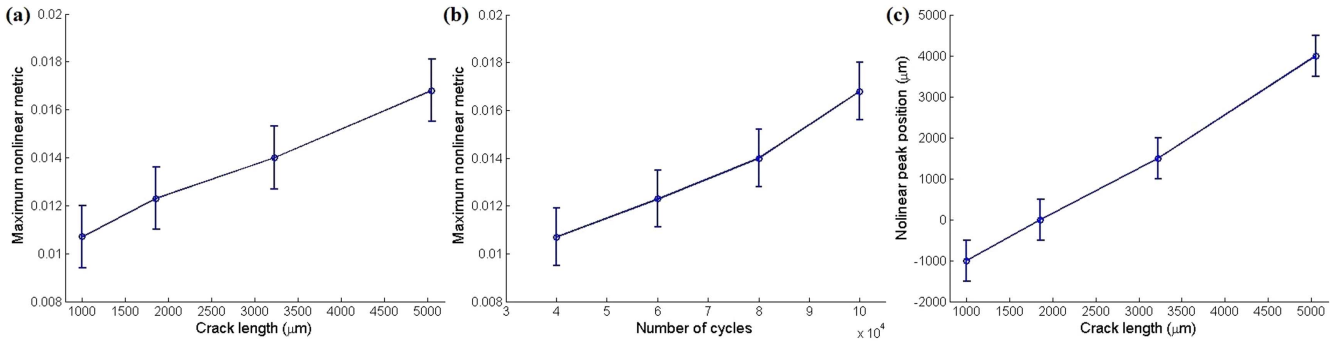

Figure 9. Maximum nonlinear metric γ during fatigue as a function of (a) actual crack length and (b) number of fatigue cycles. (c) Measured crack length from the NUI image (notch end to position of maximum nonlinear metric γ) during fatigue as a function of micrographically measured crack length (error bar represents an averaged standard deviation).

imaging, mapping out the extent of a given crack. As the same instrumentation is used, linear and nonlinear images can be produced simultaneously, and these contain complementary information. The linear images will reveal essentially geometric information from sample boundaries and large defects, whereas the NUI images will reveal nonlinear features such as partially-closed cracks and crack tips. The NUI results were obtained with the array positioned directly above the crack, an orientation that typically results in poor linear imaging as the signals reflected directly from the crack tip are small. We note however that the orientation used in NUI is beneficial as it reduces access limits relative to traditional linear array imaging (which would typically be performed as an angle inspection). The NUI technique therefore both improves sensitivity and reduces access limitations making it a viable prospect for *in situ* or permanent fatigue monitoring of, for example, pipework or pressure vessel welds.

Acknowledgments

This work was supported through the core research program within the UK Research Centre in NDE (RCNDE) funded by the Engineering and Physical Sciences Research Council (EPSRC; grant number EP/L022125/1). Data necessary to support the conclusions are included in the paper.

References

[1] Tsuda H, Lee J and Guan Y 2006 Fatigue crack propagation monitoring of stainless steel using fiber Bragg grating ultrasound sensors *Smart Mater. Struct.* **15** 1429–37
[2] Thomas R, Drinkwater B W and Liaptsis D 2005 The refection of ultrasound from partially contacting rough surfaces *J. Acoust. Soc. Am.* **117** 638–45
[3] Papazian J M *et al* 2007 Sensors for monitoring early stage fatigue cracking *Int. J. Fatigue* **29** 1668–80
[4] Nagy P B 1998 Fatigue damage assessment by nonlinear ultrasonic materials characterization *Ultrasonics* **36** 375–81
[5] Brotherhood C J, Drinkwater B W and Dixon S 2003 The detectability of kissing bonds in adhesive joints using ultrasonic techniques *Ultrasonics* **41** 521–9
[6] Su Z, Zhou C, Hong M, Cheng L, Wang Q and Qing X 2014 Acousto-ultrasonics-based fatigue damage characterization: linear versus nonlinear signal features *Mech. Syst. Signal Process.* **45** 225–39
[7] Lim H J, Song B, Park B and Sohn H 2015 Noncontact fatigue crack visualization using nonlinear ultrasonic modulation *NDT&E Int.* **73** 8–14
[8] Fierro G P M and Meo M 2015 Residual fatigue life estimation using a nonlinear ultrasound modulation method *Smart Mater. Struct.* **24** 025040
[9] Lim H J and Sohn H 2015 Fatigue crack detection using structural nonlinearity reflected on linear ultrasonic features *J. Appl. Phys.* **118** 244902
[10] Amura M, Meo M and Amerini F 2011 Baseline-free estimation of residual fatigue life using a third order acoustic nonlinear parameter *J. Acoust. Soc. Am.* **130** 1829–37
[11] Jhang K-Y 2009 Nonlinear ultrasonic techniques for non-destructive assessment of micro damage in material: a review *Int. J. Precis. Eng. Manuf.* **10** 123–35
[12] Matlack K H, Kim J-Y, Jacobs L J and Qu J 2015 Review of second harmonic generation measurement techniques for material state determination in metals *J. Nondestruct. Eval.* **34** 273
[13] Kim J-Y, Jacobs L J, Qu J and Littles J W 2006 Experimental characterization of fatigue damage in a nickel-base superalloy using nonlinear ultrasonic waves *J. Acoust. Soc. Am.* **120** 1266–73
[14] Solodov I Y and Korshak B A 2001 Instability, chaos, and 'memory' in acoustic-wave-crack interaction *Phys. Rev. Lett.* **88** 014303
[15] Cantrell J H and Yost W T 2001 Nonlinear ultrasonic characterization of fatigue microstructures *Int. J. Fatigue* **23** 487–90
[16] Averkiou M A, Roundhill D N and Powers J E 1997 A new imaging technique based on the nonlinear properties of tissues *Proc. IEEE Ultrasonics Symp.* pp 1561–6
[17] Cai A, Sun J and Wade G 1992 Imaging the acoustic nonlinear parameter with diffraction tomography *IEEE Trans. Ultrason. Ferroelectr. Freq. Control* **39** 708–15
[18] Gong X, Zhang D, Liu J, Wang H, Yan Y and Xu X 2004 Study of acoustic nonlinearity parameter imaging methods in reflection mode for biological tissues *J. Acoust. Soc. Am.* **116** 1819–25
[19] Ulrich T J, Johnson P A and Guyer R A 2007 Interaction dynamics of elastic waves with a complex nonlinear scatterer through the use of a time reversal mirror *Phys. Rev. Lett.* **98** 104301

[20] Solodov I, Wackerl J, Pfleiderer K and Busse G 2004 Nonlinear self-modulation and subharmonic acoustic spectroscopy for damage detection and location *Appl. Phys. Lett.* **84** 5386–8
[21] Ohara Y, Mihara T, Sasaki R, Ogata T, Yamamoto S, Kishimoto Y and Yamanaka K 2007 Imaging of closed cracks using nonlinear response of elastic waves at subharmonic frequency *Appl. Phys. Lett.* **90** 011902
[22] Croxford A J, Wilcox P D, Drinkwater B W and Nagy P B 2009 The use of non-collinear mixing for nonlinear ultrasonic detection of plasticity and fatigue *J. Acoust. Soc. Am.* **126** 117–22
[23] Ohara Y, Horinouchi S, Hashimoto M, Shintaku Y and Yamanaka K 2010 Nonlinear ultrasonic imaging method for closed cracks using subtraction of responses at different external loads *Ultrasonics* **51** 661–6
[24] Yan Z and Nagy P B 2000 Thermo-optical modulation for improved ultrasonic fatigue crack detection in Ti-6Al-4V *NDT&E Int.* **33** 213–23
[25] Jiao J P, Drinkwater B W, Neild S A and Wilcox P D 2009 Low-frequency vibration modulation of guided waves to image nonlinear scatterers for structural health monitoring *Smart Mater. Struct.* **18** 065006
[26] Mi B, Michaels J E and Michaels T E 2005 An ultrasonic method for dynamic monitoring of fatigue crack initiation and growth *J. Acoust. Soc. Am.* **119** 74–85
[27] Potter J N, Croxford A J and Wilcox P D 2014 Nonlinear ultrasonic phased array imaging *Phys. Rev. Lett.* **113** 144301
[28] Holmes C, Drinkwater B W and Wilcox P D 2005 Post-processing of the full matrix of ultrasonic transmit-receive array data for non-destructive evaluation *NDT&E Int.* **38** 701–11